IEEE Photonics Journal
An IEEE Photonics Society Publication

Open Access

Universal Quasi-Level Parameter for the Characterization of Laser Operation

Volume 10, Number 4, August 2018

Christian Jirauschek, ***Member, IEEE***

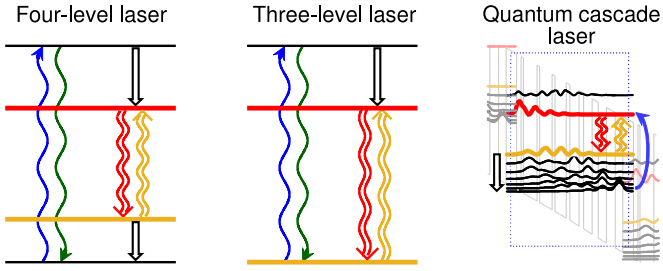

DOI: 10.1109/JPHOT.2018.2863025
1943-0655 © 2018 CCBY

IEEE photonics SOCIETY

IEEE

Universal Quasi-Level Parameter for the Characterization of Laser Operation

Christian Jirauschek, *Member, IEEE*

Department of Electrical and Computer Engineering, Technical University of Munich, D-80333 Munich, Germany

DOI:10.1109/JPHOT.2018.2863025

Manuscript received July 6, 2018; revised July 30, 2018; accepted July 31, 2018. Date of publication August 3, 2018; date of current version August 15, 2018. This work was supported in part by the German Research Foundation (DFG) and the Technical University of Munich within the funding programme Open Access Publishing, and in part by the DFG within the Heisenberg program (JI 115/4-2) and under DFG Grant JI 115/9-1. (e-mail: jirauschek@tum.de).

Abstract: A parameter is proposed which classifies the laser operating characteristics according to the quasi-level terminology, i.e., as intermediate behavior between that of an ideal two- and three-level or three- and four-level laser scheme. Since the quasi-level parameter is purely based on a generic rate equation description of the laser, no inherent assumptions about gain medium properties or the pumping process are required. The validity of the quasi-level parameter is verified for various prototypical laser schemes. As a specific example of a nonideal laser, the operating behavior of an experimental quantum cascade laser is classified, which constitutes a quite generic laser type since the active region properties can be custom-engineered by quantum design.

Index Terms: Lasers, laser theory, quantum cascade lasers.

1. Introduction

The distinction of lasers in three- and four-level schemes is of general importance for characterizing and understanding their operational behavior [1]. In particular, a three-level system where the ground level serves as both lower pump and laser level, exhibits a significantly higher lasing threshold and much stronger inversion degradation due to lasing than an otherwise equivalent four-level system. In Fig. 1, some exemplary laser schemes are illustrated, with prototypical four- and three-level schemes shown in Fig. 1(a) and Fig. 1(b), respectively. However, the behavior of lasers does not always correspond to the actual number of physical levels involved. For instance, lasers employing four levels often behave more like a three-level system, e.g., if the energy separation between the lower laser level and the lower pump level (which often coincides with the ground state) approaches or even falls below the thermal energy $k_B T$ [2], [3]. On the other hand, lasers employing only three levels can in principle exhibit four-level character, if the lower pump and laser levels are separated while the upper pump and laser levels coincide [4], as illustrated in Fig. 1(c). In general, for a given set of pump and laser levels in a gain medium, the lasing characteristics is found to lie somewhere in between a two- and a four-level behavior, and to also gradually vary with the operating parameters such as temperature [4]. As an extreme example, it has been shown that a four-level laser can gradually transform into a three- or even two-level system by decreasing the energy separation between the pump and laser states [3].

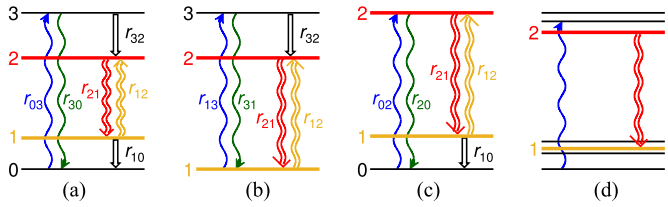

Fig. 1. Schematic of a (a) four-level system, (b) ruby-type three-level system, (c) three-level system with coinciding upper pump and laser level, and (d) system with an upper and a lower level manifold. Levels 2 and 1 are the upper (red) and lower (yellow) laser levels, and separate upper and lower pump levels are marked as 3 and 0, respectively. The transition rate between two of these levels i and j is denoted as r_{ij}.

To capture the mismatch between the number of physical levels and the lasing characteristics, the "quasi-level" terminology has been introduced where the expressions quasi-four-, three- and two-level are used to describe operating characteristics which resemble ideal four-, three- and two-level systems, respectively. This concept has been extended by developing continuous quasi-level parameters, which can also capture laser behavior in between ideal four- and three-level or three- and two-level characteristics [4]. Specifically, by dividing the energy states into an upper absorbing level manifold, comprising all the potential upper pump and laser levels, and a lower emitting one containing the lower pump and laser levels [see Fig. 1(d)], a quasi-level coefficient can be calculated based on the thermal population of the pump and laser levels within the corresponding manifolds [4], [5]. This concept is targeted at low-quantum-defect, narrowband optically pumped lasers with discrete levels, especially solid-state lasers doped with transition metal or rare earth ions where for a given pump and lasing wavelength, the levels involved are clearly specified [4].

As pointed out above, the system level terminology is of central relevance for all types of lasers, and its extension to the quasi-level concept is essential for a realistic classification of a laser's operational behavior, which rarely resembles an ideal three- or four-level system. The goal of this work is to introduce a general approach for such a quasi-level classification, which does not assume optical pumping or rely on the unambiguous identification of upper/lower manifolds or pump levels, but is directly based on the most generic description of laser gain media, i.e., the rate equation formalism for the level populations [1]. The resulting quasi-level coefficient is validated against the prototypical four-, three- and two-level cases. Furthermore, we test our approach for the possibly most generic laser type, the quantum cascade laser, where the behavior is not defined by fixed material properties, but rather the level energies and transition rates are determined by quantum engineering [6], [7]. This offers many design degrees of freedom. In particular, typically several levels are involved in the pumping process, and more than one optical transition might contribute to lasing.

2. Theoretical Model

The rate equation formalism for the level populations provides a generic description of laser gain media [1], and is widely used for a broad range of laser types [8]–[11]. The rate equations for a system with N levels can be written in the form [1]

$$\mathrm{d}_t n_k = \sum_{i \neq k} r_{ik} n_i - r_k n_k, \quad k = 1, 2, \ldots, (N-1) \tag{1a}$$

$$\sum_i n_i = n \tag{1b}$$

where n_i is the population of level i, and the conservation of the total population n is ensured by (1b). Furthermore, r_{ik} denotes the transition probability per unit time from level i to k, including both radiative and nonradiative transitions, and $r_k = \sum_{i \neq k} r_{ki}$ is the inverse lifetime of level k. The

stationary solution is found by setting $d_t = 0$, which yields

$$R\mathbf{n} = \mathbf{b}. \tag{2}$$

Here, the elements of the $N \times N$ transition rate matrix R are given by $[R]_{ii} = -r_i$ for $i = 1..(N-1)$, $[R]_{N,j} = 1$ for $j = 1..N$, and $[R]_{ij} = r_{ji}$ otherwise. Furthermore, vector $\mathbf{n}$ contains the level populations n_i, and the vector elements of $\mathbf{b}$ are given by $b_i = n\delta_{iN}$ where δ_{ij} denotes the Kronecker delta.

In the following, we assume the presence of at least three levels, and reserve $i = 2$ for the upper laser level and $i = 1$ for the lower one. As a defining criterion for three-level vs. four-level behavior of lasers, we use the change in population difference associated with an optical transition from the upper to the lower laser level: For three-level-type lasers, the upper and lower laser level occupations, n_2 and n_1, change by $\delta n_2 = -1$ and $\delta n_1 = 1$, and thus the population difference reduces by $\delta n_2 - \delta n_1 = -2$, while ideal four-level behavior is characterized by an empty lower laser level, yielding $\delta n_2 = -1$, $\delta n_1 = 0$ and thus $\delta n_2 - \delta n_1 = -1$ [5], [8]. This criterion can be quantified by the parameter

$$\gamma = \frac{\delta n_2 - (g_2/g_1)\,\delta n_1}{\delta n_2} = \frac{\delta \Delta_{21}}{\delta n_2} \tag{3}$$

where we have used the generalized espression for the inversion population

$$\Delta_{21} = n_2 - (g_2/g_1)\, n_1 \tag{4}$$

which also accounts for the statistical weights (or degeneracies) g_2 and g_1 of the upper and lower laser levels [8]. For an ideal three-level system with $g_1 = g_2$, $\gamma = 2$, while in the ideal four-level case $\gamma = 1$ [5], [8]. A link to the quasi-level terminology is then simply established by suitable linear rescaling of the parameter γ, leading to the quasi-level coefficient

$$\ell = 5 - \gamma. \tag{5}$$

Using γ, the rate equations for ideal three- and four-level lasers with fully depopulated upper pump level can be reduced to a single equation for Δ_{21} [8]:

$$d_t \Delta_{21} = -\gamma \sigma_{21} F \Delta_{21} - \tau_2^{-1} \left[\Delta_{21} + n\,(\gamma - 1)\right] + r_p\,(n - \Delta_{21})\,. \tag{6}$$

Here, σ_{21} denotes the stimulated emission cross section, and F is the photon flux, given by the ratio of optical intensity and photon energy. Furthermore, τ_2 is the non-radiative and spontaneous emission lifetime of the upper laser level, and r_p is a pump parameter, which are both related to the r_{ik} in (1a) [8]. In (6), the parametrization of the laser operating characteristics in terms of γ becomes especially apparent.

2.1 Lasers With Thermalized Manifolds

As mentioned above, the criterion defined in (3) has been applied to solid state lasers such as Nd:YAG [5], where the levels can be divided into an upper and a lower manifold [see Fig. 1(d)] with total populations n_{up} and n_{low}, respectively, and thermal distribution within each manifold. The lower laser level occupation is then obtained as $n_1 = p_1 n_{low}$ [4], [5], where $p_1 = g_1 W_1 / Z_{low}$ is the probability that an electron in the lower level manifold is actually in the lower laser level. Here, the partition function $Z_{low} = \sum_i g_i W_i$ includes all levels of the lower manifold, and $W_i = \exp\left[-E_i/(k_B T)\right]$ is the Boltzmann factor for a level i with energy E_i. Similarly, we can write $n_2 = p_2 n_{up}$ with $p_2 = g_2 W_2 / Z_{up}$. The population conservation (1b) can then be expressed as $n_1/p_1 + n_2/p_2 = n$, which directly yields $\delta n_1/\delta n_2 = -p_1/p_2$, and thus (3) gives [5]

$$\gamma = 1 + \frac{g_2}{g_1}\frac{p_1}{p_2} = 1 + \frac{Z_{up} W_1}{Z_{low} W_2}. \tag{7}$$

2.2 General Case

In the general case, where the levels cannot be divided into manifolds with thermal distributions, it is not enough to evaluate the population conservation, but the full expression (1) must be considered. The transition probability per unit time associated with stimulated photon emission is $r_{21} = \sigma_{21} F$, where for multimode operation an effective σ_{21}, obtained by averaging over the mode frequencies weighted by the relative photon flux in each mode, is used [9]. Furthermore, this process is accompanied by photon absorption transitions from level 1 to 2, with $r_{12} = (g_2/g_1)\, r_{21}$. Consequently, the stimulated emission and absorption rates per incident photon scale as $\propto \sigma_{21} n_2$ and $\propto (g_2/g_1)\, \sigma_{21} n_1$, resulting in a net generation rate $\propto \sigma_{21} \Delta_{21}$. Here, $\sigma_{21}\Delta_{21}$ directly corresponds to the net power gain coefficient if the n_i are given in units of number density. By multiplying the enumerator and denominator of (3) with σ_{21}, we see that γ can be interpreted as the ratio of changes in net generation vs stimulated emission rates per incident photon, resulting from population changes δn_2 and δn_1 due to an increased photon flux. In other words, gain saturation not only reduces stimulated emission, but for $\gamma > 1$ also increases photon reabsorption, which further decreases the net photon generation rate. Thus, the reduction in net optical gain due to gain saturation effects is γ times higher than in an otherwise equivalent laser without photon re-absorption, corresponding to the ideal four-level case.

In the following, $\delta n_{1,2}$ in (3) is derived from (2), yielding an expression for γ which only depends on the transition rate matrix R. For a flux change δF we obtain with $\delta r_{21} = \sigma_{21} \delta F$ the non-zero matrix elements $[\delta R]_{22} = -\delta r_{21}$, $[\delta R]_{12} = \delta r_{21}$, $[\delta R]_{11} = -(g_2/g_1)\, \delta r_{21}$, $[\delta R]_{21} = (g_2/g_1)\, \delta r_{21}$. The resulting change in stationary level occupations $\delta \mathbf{n}$ is found from (2) by evaluating $(R + \delta R)(\mathbf{n} + \delta \mathbf{n}) = \mathbf{b}$. Re-inserting (2) and neglecting the higher order term $\delta R \delta \mathbf{n}$, we obtain

$$R \delta \mathbf{n} = \mathbf{v} \tag{8}$$

where $\mathbf{v} = -\delta R \mathbf{n} = \Delta_{21} \delta r_{21} \mathbf{d}$, with $d_1 = -1$, $d_2 = 1$, and $d_i = 0$ otherwise. Equation (8) can for example be solved by applying Cramer's rule:

$$\delta n_i = \frac{|R_i|}{|R|} \Delta_{21} \sigma_{21} \delta F = (-1)^i \frac{|R_{1i}| + |R_{2i}|}{|R|} \Delta_{21} \sigma_{21} \delta F \tag{9}$$

where $|\ldots|$ denotes a matrix determinant and R_i is the matrix formed by replacing the i-th column of R by vector $\mathbf{d}$. The last expression is obtained by the Laplace expansion, where R_{ij} denotes the $(N-1) \times (N-1)$-matrix that results from R by removing the ith row and the jth column. From (3), we then obtain with (9)

$$\gamma = 1 - \frac{g_2}{g_1} \frac{|R_1|}{|R_2|} = 1 + \frac{g_2}{g_1} \frac{|R_{11}| + |R_{21}|}{|R_{12}| + |R_{22}|}. \tag{10}$$

Above formulation of γ, based on infinitesimal population changes δn_i from the stationary values n_i, accounts for the fact that the laser characteristics in general depends on the chosen operating point, and can gradually vary with, e.g., the pumping strength. Notably, γ in (10) does not depend on the intensity of the laser radiation (apart from possible secondary changes of the other rate coefficients r_{ij}) since stimulated emission and absorption rates are affected in equal measure, and thus does not vary with the intensity distribution of the laser beam or related parameters such as the field overlap or beam quality factor. On the other hand, for spatially inhomogeneous pumping as particularly occurs in solid state and fiber lasers, the pump rates in (2) are position dependent, and thus also the quasi-level coefficient (10) varies in principle with the position in the gain medium. The dependence on the transverse pump profile is typically eliminated by integrating the rate equations over the transverse plane, subsuming the radial pump power distribution into an effective mode area, overlap factor and average doping density [9]. Also, as discussed in Section 2.1, solid state and fiber lasers can often be described by the simplified expression (7) for thermalized upper and lower manifolds, which does not depend on the pump rate anymore and thus results in a position independent γ.

3. Validation for Prototypical Three- and Four-Level Schemes

In Fig. 1(a)–(c), prototypical three- and four-level schemes are illustrated, and the dominant transitions with their corresponding rates r_{ij} are indicated. In the following, these idealized schemes are used as test cases to validate (10). For the three-level scheme shown in Fig. 1(b), with the ruby gain medium as its most prominent representative, the lower pump and laser levels coincide. Considering all possible transitions, (10) yields

$$\gamma = 1 + \frac{g_2}{g_1}\frac{r_{31} + r_{32} + r_{23}}{r_{31} + r_{32} + r_{13}}. \tag{11}$$

To obtain lasing, the filling of the upper laser level 2 from pump level 3 has to be efficient, i.e., $r_{32} \gg r_{23}$ as also indicated in Fig. 1(b), and strong enough to keep the upper pump level nearly empty, $r_{32} \gg r_{13}$. Since furthermore for the pump transition, r_{31}/r_{13} is of order unity or less, (11) and (5) yield $\gamma = 1 + g_2/g_1$ and $\gamma = 4 - g_2/g_1$ in agreement with literature [8]. Specifically, for $g_1 = g_2$, $\gamma = 2$ and $\ell = 3$, as expected for an ideal three-level laser. Also the gradual transformation into a quasi-two-level system is captured by our model. For small energy separation between the upper pump and laser level, the population of level 2 approaches thermal equilibrium with that of 3, and $r_{32} \approx r_{23}$. Under this condition, above result for an ideal three-level laser changes to $\gamma \approx 1 + (r_{32} + r_{23})/r_{32} \approx 3$ and consequently $\ell \approx 2$, which indicates quasi-two-level behavior as expected [3].

In reality, the ruby laser ground level has a statistical weight $g_1 = 4$, and there are two upper laser levels at 1.7870 eV and 1.7906 eV, respectively, with $g_2 = 2$ for each level. The close level spacing gives rise to a thermal distribution with an occupation of $\approx n_2/2$ in both upper laser levels. However, due to the slightly higher Boltzmann occupation probability of the one at 1.7870 eV, lasing naturally occurs only between this level and the ground state. The effective change in upper laser level population δn_2 in (3) must thus be replaced by $\delta n_2/2$. Since on the other hand also $g_2/g_1 = 1/2$, we again recover above result for ruby-type three-level lasers, $\gamma = 2$. This underlines the necessity to consider the statistical weights in the definition of γ in (3).

A further type of three-level system is obtained for coinciding upper pump and laser levels, as shown in Fig. 1(c). This situation applies for example to a Nd:YAG laser if pumped at 886 nm [4]. In analogy to (11), we obtain

$$\gamma = 1 + \frac{g_2}{g_1}\frac{r_{01} + r_{02} + r_{20}}{r_{01} + r_{02} + r_{10}}. \tag{12}$$

For a good laser, we can expect pumping from ground state 0 into the upper rather than the lower laser level, $r_{02} \gg r_{01}$, see Fig. 1(c), and rapid depopulation of the lower laser level to keep it approximately empty, $r_{10} \gg r_{02}$. Since furthermore for the pump transition, r_{20}/r_{02} is of order unity or less, (12) and (5) yield $\gamma = 1$ and $\ell = 4$. This result might be counterintuitive at first sight, but agrees with previous findings that lasing operation in such a three-level medium exhibits four-level character [4]. The underlying reason is that efficient lower laser level depopulation is obtained by separating it from the ground level, while the upper laser level is depopulated by the lasing action which avoids saturation of the pumping process [4].

For a four-level system as shown in Fig. 1(a), (10) yields

$$\gamma = 1 + \frac{g_2}{g_1}\frac{f_{2,1,0,3} + f_{2,1,3,0}}{f_{1,2,0,3} + f_{1,2,3,0}} \tag{13}$$

with

$$f_{i,j,k,l} = r_{ik}\left(r_{kl} + r_l\right) + r_{ki}\left(r_l - \frac{r_{li}}{2}\right) + r_{kj}\left(r_{lk} + \frac{r_{lj}}{2}\right). \tag{14}$$

As for the ruby-type three-level laser, the filling of the upper laser level 2 from pump level 3 has to be efficient and strong enough to keep the upper pump level nearly empty, i.e., $r_{32} \gg r_{31}, r_{23}, r_{13}, r_{03}$. Furthermore for the pump transition, r_{30}/r_{03} is of order unity or less. Under these conditions, (13) simplifies to $\gamma \approx 1 + (g_2/g_1)(r_0 + r_{20})/(r_0 + r_{10})$, where for the lower pump level transitions to the upper pump level dominate, i.e., $r_0 \approx r_{03}$. Assuming rapid depopulation of the lower laser level to

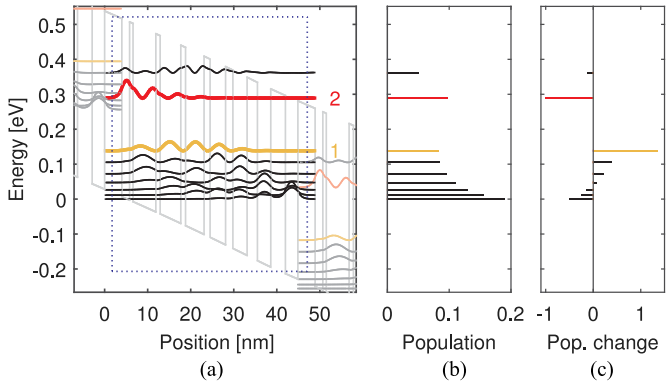

Fig. 2. (a) Conduction band profile with energy levels and wavefunctions squared of the investigated QCL. The rectangle denotes a single QCL stage. The main upper and lower laser levels are marked by red and yellow lines, respectively. (b) Relative level populations $n_i / \sum_k n_k$ at operating bias, and (c) population changes δn_i (normalized to $|\delta n_2|$) associated with an increased photon flux.

keep its population low, $r_{10} \gg r_0, r_{20}$, we obtain $\gamma = 0$ and thus $\ell = 4$ as expected [8]. Notably, r_{21} and r_{12} do not show up in (11)–(14), i.e., the obtained expression for γ is independent of the lasing strength (apart from possible secondary changes of the other rate coefficients r_{ij}).

4. Exemplary Application to Quantum Cascade Laser

In the following, we use our approach to investigate the operational behavior of an examplary non-ideal laser. Here we choose a quantum cascade laser (QCL), which is based on electron transitions between quantized energy levels in the conduction band of a semiconductor multiple quantum well structure. The QCL is one of the most generic laser types since the operating characteristics is not primarily given by the properties of the used materials, but rather the states and associated transition rates can be engineered by quantum design of the nanostructured active region [6], [7]. This opens up a plethora of design options, involving discrete levels as well as minibands consisting of a quasi-continuum of states. QCLs feature a periodic arrangement of stages, each containing a laser transition, and thus each electron can undergo multiple photon emission processes. Pumping is achieved by electron injection into the upper laser level of the subsequent stage. Despite their unconventional operating principle, QCLs are often described by a rate equation model, demonstrating the versatility of this approach [11], [12]. Specifically, by considering adequate periodic boundary conditions, the QCL can be described by an effective rate equation of the form (1) for the levels of a single representative stage [13].

Here we choose an experimental room temperature QCL structure emitting at 8.5 μm [14]. The energy levels of a representative stage are shown in Fig. 2(a). The QCL is a bound-to-continuum design which combines an isolated upper laser level 2 with a quasi-continuum of states. This so-called miniband contains the lower laser level 1, the injector states which effectively act as upper pump levels by injecting electrons into the upper laser level of the next stage, and additional states for the depopulation of the lower laser level and electron transport to the injector states. In the following, we show that while descriptions based on thermalized level manifolds are here not applicable, the quasi-level parameter introduced in (10) also works for this highly unconventional laser. The corresponding elements of matrix R are obtained from a density matrix Monte Carlo simulation, where the relevant scattering, optical and tunneling rates are self-consistently evaluated based on the underlying Hamiltonians, without using empirical or fitting parameters [13], [15]–[17]. At an applied bias of 57 kV/cm where the peak optical output power ($\sim$1.1 W) and maximum current density ($\sim$4.1 kA/cm^2) was experimentally measured [14], our simulation yields 1.02 W and 4.11 kA/cm^2 in very close agreement, thus confirming the validity of the theoretical data. Figure 2(b) shows the level populations, as obtained by solving (2) or directly from the density matrix Monte

Carlo simulation. Equation (8) provides the change in level populations associated with an increased photon flux, see Fig. 2(c). From (10) and (5), we obtain $\gamma = 2.35$ and thus a quasi-level coefficient $\ell = 2.65$. This result can be explained by inspection of Fig. 2(c): An increased photon flux causes a significant filling of the lower laser level 1, while the population increase of the miniband states directly below is far less pronounced. This indicates that the depopulation of the lower laser level is only moderately efficient, exhibiting three-level rather than four-level characteristics. On the other hand, the population of the lowest miniband states, which inject electrons into the upper laser level of the next stage, gets clearly reduced. This indicates that in contrast to ideal four- or three-level systems [see Figs. 1(a) and 1(b)], after the emission process, the electron is not immediately available for re-injection into the upper laser level. Consequently, the lasing characteristics lies in between two- and three-level behavior as indicated by $2 < \ell < 3$. This situation is also often observed for solid state lasers [4], where the laser and pump states can be considered part of upper and lower level manifolds with thermal distributions, and thus (7) can be used [5]. However, this approximate treatment fails for the QCL investigated here: Associating the miniband with the lower manifold, (7) would with $p_1/p_2 \ll 1$ [see Fig. 2(b)] yield an erroneous value of γ close to 1. The reason is that although the populations n_i in the miniband might somewhat resemble a thermal distribution [see Fig. 2(b)], the relative population change $\delta n_i/n_i$ associated with an increased photon flux is not equal for the different miniband levels as would be the case for thermal equilibrium (see Section 2.1), but rather varies in magnitude and sign.

5. Model Extension to Multiple Lasing Transitions

Frequently, more than one transition has a considerable cross section at the lasing frequency. The case of multiple lasing transitions between distinct levels can again be described by (2), now with several lower and upper laser levels $l = 1..l_{\max}$ and $u = (l_{\max}+1)..(l_{\max}+u_{\max})$. We again interpret γ as the ratio of changes in net gain vs "pure" gain without reabsorption, resulting from population changes $\delta n_{u,l}$ due to gain saturation effects (see Section 2.2). If the n_i are in units of number density, the net and pure power gain coefficients are directly given by $\sum_{u,l}\sigma_{ul}\Delta_{ul}$ and $\sum_{u,l}\sigma_{ul}n_u$, where we sum over all lasing transitions $u \to l$ with non-negligible emission cross sections σ_{ul}. Using $\Delta_{ul} = n_u - (g_u/g_l)\,n_l$, we obtain

$$\gamma = \frac{\sum_{ul}\sigma_{ul}\delta\Delta_{ul}}{\sum_{ul}\sigma_{ul}\delta n_u} = 1 - \frac{\sum_{ul}\sigma_{ul}(g_u/g_l)\,\delta n_l}{\sum_{ul}\sigma_{ul}\delta n_u}. \tag{15}$$

Equation (15) can also be written as $\gamma = \sum_{ul}\gamma_{ul}$ with $\gamma_{ul} = \sigma_{ul}\delta\Delta_{ul}/\sum_{u'l'}\sigma_{u'l'}\delta n_{u'}$ to break down the contributions of the individual transitions, which are however generally coupled by cross-saturation effects, see (17) below.

The consistency with (3) for an upper laser level 2 with degeneracy g_2 and a lower laser level 1 with degeneracy g_1 can easily be checked by representing level 2 as g_2 individual upper laser levels u with $g_u = 1$, and level 1 as g_1 individual lower laser levels l with $g_l = 1$. For an occupation change δn_2 due to optical transitions, the change in each individual level u is then given by $\delta n_u = \delta n_2/g_2$, and analogously we obtain $\delta n_l = \delta n_1/g_1$. Inserting δn_u and δn_l into (15) and summing over all $g_1 g_2$ possible transitions between levels u and l, where we assume identical emission cross sections σ_{ul}, we recover (3).

5.1 Lasers With Thermalized Manifolds

The case of closely spaced levels which cannot be spectroscopically resolved, such as Stark manifolds in solid-state gain media, can be treated in analogy to Section 2.1. We assume that the levels can be divided into an upper and a lower manifold with total populations n_{up} and n_{low}, with thermal distributions within each manifold. The upper and lower laser level populations are then given by $n_u = p_u n_{\text{up}}$ with $p_u = g_u W_u/Z_{\text{up}}$ and $n_l = p_l n_{\text{low}}$ with $p_l = g_l W_l/Z_{\text{low}}$. Consequently, the population changes are $\delta n_u = p_u \delta n_{\text{up}}$ and $\delta n_l = p_l \delta n_{\text{low}}$ where $\delta n_{\text{up}} = -\delta n_{\text{low}}$ follows from population

conservation (1b). Inserting these expressions in (15), we can write the result as

$$\gamma = 1 + \frac{\sum_{ul} g_u \left(\sigma_{ul}/g_l\right) p_l}{\sum_{ul} g_l \left(\sigma_{ul}/g_l\right) p_u}. \tag{16}$$

The sums in the enumerator and denominator correspond to the expressions for the so-called spectroscopic absorption and emission cross sections σ_a and σ_e, i.e., the quantities that are accessible to direct external measurements [18]. Thus (16) can simply be written as $\gamma = 1 + \sigma_a/\sigma_e$ in agreement with literature [19].

5.2 General Case

For a given transition $u \rightarrow l$, a flux change δF introduces a change in transition rate $\delta r_{ul} = \sigma_{ul}\delta F$, yielding non-zero matrix elements $[\delta R]_{uu} = -\delta r_{ul}$, $[\delta R]_{lu} = \delta r_{ul}$, $[\delta R]_{ll} = -\left(g_u/g_l\right)\delta r_{ul}$, $[\delta R]_{ul} = \left(g_u/g_l\right)\delta r_{ul}$. For more than one optical transition, δR is obtained by summing up the individual contributions. The population changes $\delta n_{u,l}$ in (15) can then be obtained from the stationary rate equation (8). In analogy to (9), we obtain

$$\delta n_i = \frac{\delta F}{|R|} \sum_{ul} \sigma_{ul} \Delta_{ul} \left[(-1)^{u+i} \left|R_{ui}\right| - (-1)^{l+i} \left|R_{li}\right| \right] \tag{17}$$

where we sum over all optical transitions $u \rightarrow l$ from an upper laser level u to a lower one l with non-negligible cross sections σ_{ul}.

5.2.1 Exemplary Application to Quantum Cascade Laser: We apply this generalized analysis to the QCL in Fig. 2(a), where in addition to the main lasing transition $2 \rightarrow 1$, we take into account lasing from level 2 to the second- and third-highest miniband levels, as well as various loss transitions. Although the cross sections σ_{ul} of these additional transitions are all below 10% of σ_{21}, their summed-up contributions somewhat affect the operating characteristics. With (17), (15) and (5) we now obtain $\gamma = 2.10$ and $\ell = 2.90$, indicating a slight improvement in the quasi-level behavior from $\ell = 2.65$ obtained above. We attribute this to the inclusion of the additional lower laser levels in (15), increasing the number of available final states for laser emission. This positive effect of multiple lower laser levels becomes most evident in the limiting case of degeneracy, where (3) yields $\gamma \approx 1$ for $g_1 \gg g_2$, indicating that the laser approaches quasi-four-level behavior.

6. Conclusions

In conclusion, we have introduced a general quasi-level parameter for classifying the laser operating characteristics by comparison to prototypical four-, three- and two-level behavior. This parameter can also capture intermediate behavior and is applicable to any laser which can be described by a generic rate equation model for the level populations. We have verified the validity of the quasi-level parameter for various prototypical laser schemes. As a specific example of a non-ideal laser, we have applied our approach to an experimental quantum cascade laser which offers high design flexibility due to its reliance on quantum engineered transitions. Here we have chosen a bound-to-continuum design which employs optical transitions from an isolated upper level to a miniband, consisting of a quasi-continuum of states. We have demonstrated that conventional definitions of quasi-level parameters fail in this case because they rely on a thermal electron distribution in the level manifolds, while our approach based on generic rate equations yields meaningful results.

References

[1] A. E. Siegman, *Lasers*. Herndon, VA, USA: University Science Books, 1986.
[2] T. Fan and R. L. Byer, "Modeling and CW operation of a quasi-three-level 946 nm Nd: YAG laser," *IEEE J. Quantum Electron.*, vol. QE-23, no. 5, pp. 605–612, May 1987.
[3] J. Hewitt, J. Readle, and J. Eden, "Observation of the continuous transformation of a four level laser into a two level system," *Appl. Phys. Lett.*, vol. 101, 2012, Art. no. 071102.

[4] J. O. White, "Parameters for quantitative comparison of two-, three-, and four-level laser media, operating wavelengths, and temperatures," *IEEE J. Quantum Electron.*, vol. 45, no. 10, pp. 1213–1220, Oct. 2009.
[5] N. P. Barnes, B. M. Walsh, R. L. Hutcheson, and R. W. Equall, "Pulsed $^4F_{3/2}$ to $^4I_{9/2}$ operation of Nd lasers," *J. Opt. Soc. Amer. B*, vol. 16, pp. 2169–2177, 1999.
[6] J. Faist, F. Capasso, D. L. Sivco, C. Sirtori, A. L. Hutchinson, and A. Y. Cho, "Quantum cascade laser," *Science*, vol. 264, pp. 553–556, 1994.
[7] J. Faist, *Quantum Cascade Lasers*. Oxford, U.K.: Oxford Univ. Press, 2013.
[8] W. Koechner, *Solid-State Laser Engineering*. Berlin, Germany: Springer, 2013.
[9] C. Barnard, P. Myslinski, J. Chrostowski, and M. Kavehrad, "Analytical model for rare-earth-doped fiber amplifiers and lasers," *IEEE J. Quantum Electron.*, vol. 30, no. 8, pp. 1817–1830, Aug. 1994.
[10] C. B. Moore, R. E. Wood, B.-L. Hu, and J. T. Yardley, "Vibrational energy transfer in CO_2 lasers," *J. Chem. Phys.*, vol. 46, pp. 4222–4231, 1967.
[11] D. Indjin, P. Harrison, R. W. Kelsall, and Z. Ikonić, "Self-consistent scattering theory of transport and output characteristics of quantum cascade lasers," *J. Appl. Phys.*, vol. 91, pp. 9019–9026, 2002.
[12] L. Schrottke, X. Lü, and H. Grahn, "Fourier transform-based scattering-rate method for self-consistent simulations of carrier transport in semiconductor heterostructures," *J. Appl. Phys.*, vol. 117, 2015, Art. no. 154309.
[13] C. Jirauschek and T. Kubis, "Modeling techniques for quantum cascade lasers," *Appl. Phys. Rev.*, vol. 1, 2014, Art. no. 011307.
[14] A. Bismuto, R. Terazzi, M. Beck, and J. Faist, "Electrically tunable, high performance quantum cascade laser," *Appl. Phys. Lett.*, vol. 96, 2010, Art. no. 141105.
[15] A. Mátyás, P. Lugli, and C. Jirauschek, "Photon-induced carrier transport in high efficiency midinfrared quantum cascade lasers," *J. Appl. Phys.*, vol. 110, 2011, Art. no. 013108.
[16] C. Jirauschek, "Monte Carlo study of carrier-light coupling in terahertz quantum cascade lasers," *Appl. Phys. Lett.*, vol. 96, 2010, Art. no. 011103.
[17] C. Jirauschek, "Density matrix Monte Carlo modeling of quantum cascade lasers," *J. Appl. Phys.*, vol. 122, 2017, Art. no. 133105.
[18] M. Eichhorn, *Laser Physics: From Principles to Practical Work in the Lab*. Berlin, Germany: Springer, 2014.
[19] J. I. Mackenzie, J. W. Szela, S. J. Beecher, T. L. Parsonage, R. W. Eason, and D. P. Shepherd, "Crystal planar waveguides, a power scaling architecture for low-gain transitions," *IEEE J. Sel. Topics Quantum Electron.*, vol. 21, no. 1, pp. 380–389, Jan./Feb. 2015.